



## PAPER

## Spatially confined responses of mouse visual cortex to intracortical magnetic stimulation from micro-coils

RECEIVED  
27 July 2020REVISED  
17 September 2020ACCEPTED FOR PUBLICATION  
30 September 2020PUBLISHED  
21 October 2020Sang Baek Ryu<sup>1</sup> , Angeliq ue C Paulk<sup>2</sup>, Jimmy C Yang<sup>1,2</sup>, Mehran Ganji<sup>3</sup>, Shadi A Dayeh<sup>3</sup>, Sydney S Cash<sup>2</sup>, Shelley I Fried<sup>1,4</sup> and Seung Woo Lee<sup>1,5</sup> <sup>1</sup> Department of Neurosurgery, Massachusetts General Hospital and Harvard Medical School, Boston, MA, United States of America<sup>2</sup> Department of Neurology, Massachusetts General Hospital and Harvard Medical School, Boston, MA, United States of America<sup>3</sup> Department of Electrical and Computer Engineering, University of California San Diego, La Jolla, CA, United States of America<sup>4</sup> Boston VA Healthcare System, Boston, MA, United States of AmericaE-mail: [Lee.Seungwoo@mgh.harvard.edu](mailto:Lee.Seungwoo@mgh.harvard.edu)**Keywords:** micro-magnetic stimulation, implantable micro-coil, primary visual cortex, micro-electrocorticography ( $\mu$ -ECoG), visual prosthesis**Abstract**

*Objective.* Electrical stimulation via microelectrodes implanted in cortex has been suggested as a potential treatment for a wide range of neurological disorders. Despite some success however, the effectiveness of conventional electrodes remains limited, in part due to an inability to create specific patterns of neural activity around each electrode and in part due to challenges with maintaining a stable interface. The use of implantable micro-coils to magnetically stimulate the cortex has the potential to overcome these limitations because the asymmetric fields from coils can be harnessed to selectively activate some neurons, e.g. vertically-oriented pyramidal neurons while avoiding others, e.g. horizontally-oriented passing axons. *In vitro* experiments have shown that activation is indeed confined with micro-coils but their effectiveness in the intact brain of living animals has not been evaluated. *Approach.* To assess the efficacy of stimulation, a 128-channel custom recording microelectrode array was positioned on the surface of the visual cortex (ECoG) in anesthetized mice and responses to magnetic and electric stimulation were compared. Stimulation was delivered from electrodes or micro-coils implanted through a hole in the center of the recording array at a rate of 200 pulses per second for 100 ms. *Main results.* Both electric and magnetic stimulation reliably elicited cortical responses, although activation from electric stimulation was spatially expansive, often extending more than 1 mm from the stimulation site, while activation from magnetic stimulation was typically confined to a  $\sim 300\ \mu\text{m}$  diameter region around the stimulation site. Results were consistent for stimulation of both cortical layer 2/3 and layer 5 as well as across a range of stimulus strengths. *Significance.* The improved focality with magnetic stimulation suggests that the effectiveness of cortical stimulation can be improved. Improved focality may be particularly attractive for cortical prostheses that require high spatial resolution, e.g. devices that target sensory cortex, as it may lead to improved acuity.

**1. Introduction**

Electric stimulation has been used to probe structure and function of the cortex (Mandonnet *et al* 2010, Borchers *et al* 2011, Keller *et al* 2014) and is also being evaluated to treat impaired or lost function in a wide array of applications (Normann *et al* 2009, Bensmaia and Miller 2014, Lewis *et al* 2015). For example, electric stimulation of the visual

system has led to many fundamental insights about cortical visual structure and function (Tolias *et al* 2005, Logothetis *et al* 2010). Electric stimulation of the cortex also leads to visual sensations (phosphenes), and remains under active investigation for its potential to restore sight to the blind (Schmidt *et al* 1996, Normann *et al* 2009, Tehovnik *et al* 2009, Beauchamp *et al* 2020). Stimulation of somatosensory cortex is also being investigated as a way to provide tactile sensation to users of brain machine interfaces (Flesher *et al* 2016). Several fundamental

<sup>5</sup> Author to whom any correspondence should be addressed.

limitations raise concerns about the long-term viability of implantable electrodes however. For example, the insertion of electrodes into the cortex induces a wide range of adverse biological reactions, including inflammatory responses that can lead to glial scarring and encapsulation of the electrode. This can alter the spatial spread of the electric fields induced by stimulation and may result in decreased effectiveness (Polikov *et al* 2005, Grill *et al* 2009, Davis *et al* 2012). Another important limitation of electrodes is that they typically activate all nearby neurons and neuronal processes. Thus, in the cortex for example, vertically oriented pyramidal neurons are generally considered to be a desirable target of stimulation but horizontally-oriented processes, including the passing axons of distal neurons, get activated as well. This causes activation to spread beyond the local region of the stimulating electrode and can diminish the effectiveness of stimulation, especially in applications that target sensory cortex, i.e. where the ability to create spatially and temporally precise neural activity is thought to be essential to optimizing functionality of the implant. In theory, an implant that precisely replicated the patterns of neural activity that normally arise physiologically in the healthy system would be the most effective, but this is challenging given the high density of cells in the cortex as well as the diversity of cell types.

Recent studies suggest that magnetic stimulation induced by implantable micro-coils may allow for better control over neuronal activation (Lee *et al* 2016, 2019). Unlike the fields generated by electrodes, the electric fields induced by magnetic stimulation are spatially asymmetric and therefore exert stronger driving forces for activation along some orientations than others. In the cortex, this means that vertically-oriented pyramidal neurons located close to the coil can be selectively targeted without simultaneously targeting horizontally oriented passing axons (Lee *et al* 2016, 2019, Lee and Fried 2017). As a result, the spatial extent of activation is better confined with coils than with micro-electrodes. Another potential advantage of micro-coils is that magnetic fields pass readily through biological materials and thus are less susceptible to changes in the impedance of the tissue surrounding the implant. As a result, the patterns of activation are likely to remain more stable over time with coils. In addition, inductive activation eliminates the delivery of electrical charge directly into the brain and thus greatly reduces a host of safety concerns, further enhancing the stability of performance over time. Finer control of activation and enhanced stability suggest coil-based devices may be useful in next-generation cortical implants. However, previous testing of micro-coils has largely been limited to brain slices *in vitro* and thus the effectiveness of coils in the intact cortex has not been well explored. Some studies have explored the response of auditory cortex to magnetic stimulation but the devices used in these

studies were non-penetrating (Osanai *et al* 2018), and are too large to be incorporated into multi-channel arrays that would be suitable for sensory implants (Minusa *et al* 2018).

Here, we measured the cortical response to magnetic stimulation induced by a micro-coil implanted into mouse visual cortex; results were compared to identical experiments with an implanted micro-electrode. A custom-made 128-channel ECoG recording array (Ganji *et al* 2019, Paulk *et al* 2019) was used to capture responses from the cortical surface and the wide extent of the array allowed the full spread of activation to be assessed. A hole in the center of the array allowed an electrode to be inserted and subsequently replaced with a micro-coil so that responses to both electrical and magnetic stimulation could be directly compared.

## 2. Materials and methods

### 2.1. PEDOT:PSS recording array design and fabrication

A custom microelectrode array was fabricated for use in recording of micro-electrocorticography ( $\mu$ -ECoG). The  $\mu$ -ECoG array consists of 128 electrodes that are radially arranged in seven concentric circular rings (figures 1(A) and (B)). The diameter of each electrode is 30  $\mu\text{m}$ ; and the array has a through hole (diameter: 250  $\mu\text{m}$ ) in the center. Average distances of electrodes in each ring, from the center of array, are 172  $\mu\text{m}$ , 275  $\mu\text{m}$ , 448  $\mu\text{m}$ , 670  $\mu\text{m}$ , 1048  $\mu\text{m}$ , 1450  $\mu\text{m}$  and 1950  $\mu\text{m}$ . The electrodes were coated with a conductive polymer, poly (3,4-ethylenedioxythiophene) polystyrene sulfonate (PEDOT:PSS), which has low impedance and high charge injection capacity. The fabrication of the PEDOT:PSS recording array is similar to previously established protocols (Uguz *et al* 2016, Ganji *et al* 2017, 2018). Silicon (Si) wafers were used as substrate carriers for deposition of parylene-C layers. The Si substrates were first cleaned with acetone/isopropanol (IPA)/deionized (DI) water/IPA, which was then followed by ultrasonic agitation in IPA for 5 min. To facilitate detachment of the device after the process was completed, diluted Micro-90 (0.1%)—an anti-adhesion layer—was spun-cast at 1500 rpm on the substrate. A first parylene-C layer ( $\sim 10$   $\mu\text{m}$ ) was deposited by chemical vapor deposition using a parylene deposition system 2010. Prior to metallization, metal lead patterns were defined using a Karl Suss MA6 mask aligner using NR9-3000 negative resist and subsequently developed. 15 nm chromium (Cr) adhesion layer and 100 nm gold (Au) contact layer were then deposited using Temescal bell jar deposition 1800 electron beam evaporator, and metal leads were defined by a lift-off process in acetone. Then, patterns of the contact sites were defined using NR9-6000 negative resist and a Karl Suss MA6 mask aligner for exposure. A lift-off process in acetone followed shortly after.  $\text{O}_2$  plasma

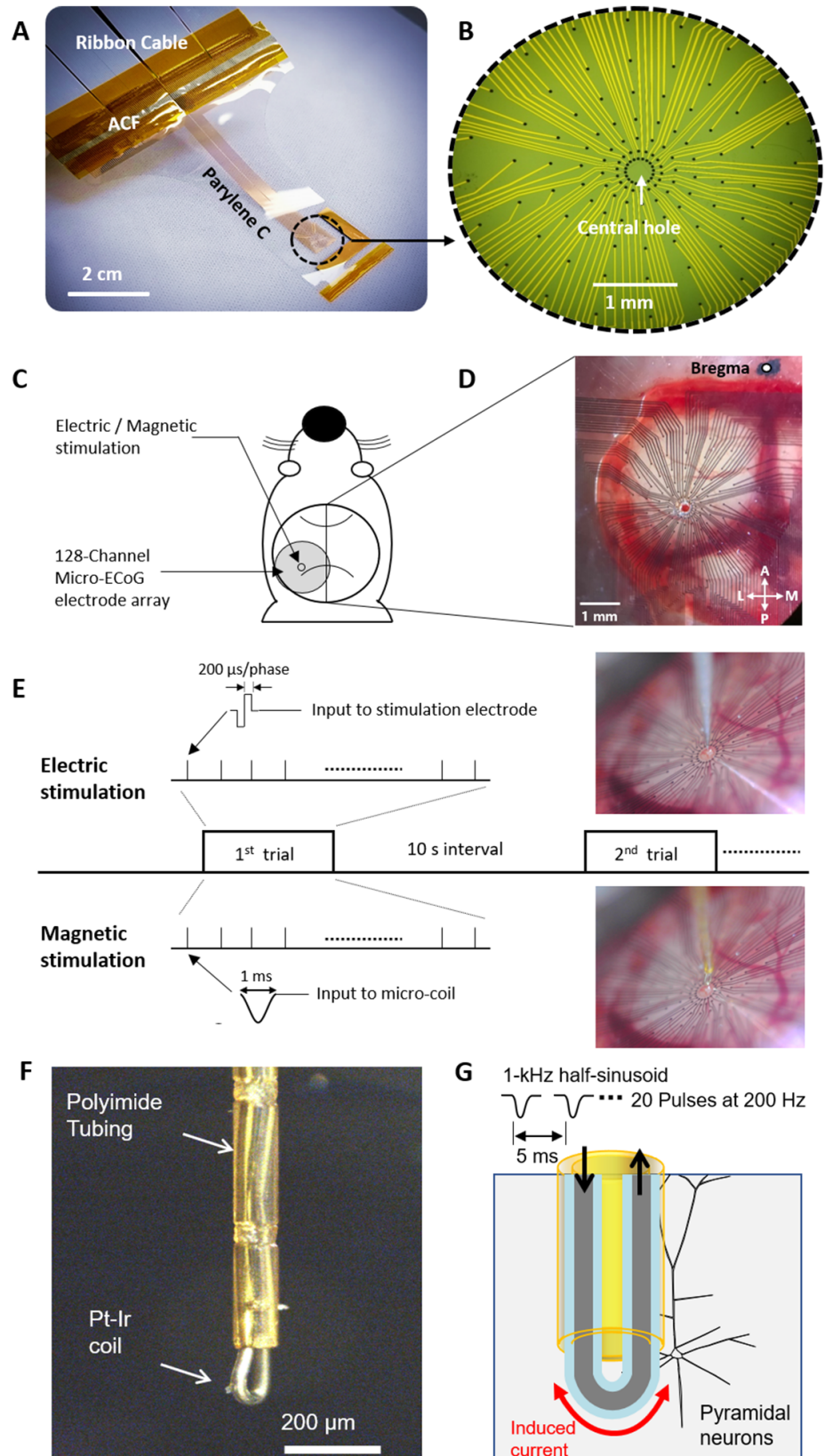


**Figure 1.** Micro-ECoG ( $\mu$ -ECoG) field potential recording from the primary visual cortex (V1) of the mouse. (A, B) Photograph of the  $\mu$ -ECoG PEDOT:PSS recording array. The central hole (diameter:  $\sim 250 \mu\text{m}$ ) allowed coils or electrodes to be inserted into cortex; the 128-channel recording electrodes (diameter:  $30 \mu\text{m}$ ) were arranged in seven concentric rings. The diameter of the outermost ring was 4 mm. (C) Schematic of the array centered over V1 of the left hemisphere. (D) Photograph of the array situated over V1 (A: anterior; L: lateral; P: posterior; M: medial). (E) Stimulation paradigm for electric and magnetic stimulation. One trial consisted of 20 pulses delivered at a repetition rate of 200 pulses per second. Each stimulation trial was repeated 20 times with a 10 s interval between trials. Right panels show an electrode (top) and micro-coil (bottom) inserted through the center hole of the array. (F) Schematic of the U-shape micro-coil (G) Conceptual diagram of intracortical magnetic stimulation using a micro-coil.

(Oxford Plasmalab 80 reactive ion etching) was then applied for 2 min (150 W radio frequency (RF) power) to activate the surface of parylene-C for enhancing the adhesion of the subsequent encapsulating parylene-C layer. A layer of 1.9–2.5  $\mu\text{m}$  parylene-C was then deposited and followed by coating another Micro 90 anti-adhesion layer with slightly higher concentrated Micro-90 (1% as opposed to 0.1% for the first layer) to facilitate the separation of the subsequent layers. Then a third parylene-C layer was deposited as sacrificial layer. To define the patterns on electrode sites, a thick 2010 SU-8 photoresist layer was exposed and developed using Karl Suss MA6 mask aligner and SU8 developer. Prior to deposition of PEDOT:PSS film,  $\text{O}_2$  plasma was used to etch the openings in the third and second parylene-C layers all the way to the contact sites. Additionally, a hole at the center of the circular array was etched through all parylene C layers. 20 ml aqueous dispersion of PEDOT:PSS (PH 1000 from Clevios) was mixed with ethylene glycol (5 ml), dodecylbenzene sulfonic acid (DBSA, 50  $\mu\text{l}$ ), and 1 wt% of (3-glycidioxypropyl) trimethoxysilane (GOPS), and the solution was spun-cast at 650 rpm for 30 s and prebaked at 95  $^\circ\text{C}$  for 1 min. Then, to define the PEDOT:PSS film on top contact sites, the sacrificial parylene-C layer was mechanically peeled off. Finally, the arrays were cured at 140  $^\circ\text{C}$  for 1 h and then immersed in DI water to remove any Micro-90 residue from the array surface.

## 2.2. Animal preparation

Experiments were performed on 11 adult (age 2–8 months) male C57BL/6 mice (The Jackson Laboratory, USA). This study was carried out in accordance with the recommendations of all federal and institutional guidelines. The protocol was approved by the Institutional Animal Care and Use Committee of the Massachusetts General Hospital (MGH). The mice were housed in the animal facility of MGH under a 12-hour light/dark cycle. Each mouse was anesthetized by an intraperitoneal injection of a mixture of Ketamine (100 mg  $\text{kg}^{-1}$ , Henry Schein Animal Health, USA) and Xylazine (10 mg  $\text{kg}^{-1}$ , Akorn Inc. USA). Body temperature was maintained at 37.5  $^\circ\text{C}$  by a heating pad. The depth of anesthesia was evaluated every 30–60 min by testing the paw withdrawal reflex, the eyelid reflex and whisker movements; Ketamine (100 mg  $\text{kg}^{-1}$ , ~50% of the initial Ketamine-Xylazine dose) was redosed as needed. For the post-mortem experiment, the animal was euthanized by anesthetic overdose by an intraperitoneal injection of a mixture of Ketamine (300 mg  $\text{kg}^{-1}$ , Henry Schein Animal Health, USA) and Xylazine (30 mg  $\text{kg}^{-1}$ , Akorn Inc., USA).

## 2.3. Surgical procedure and data recording

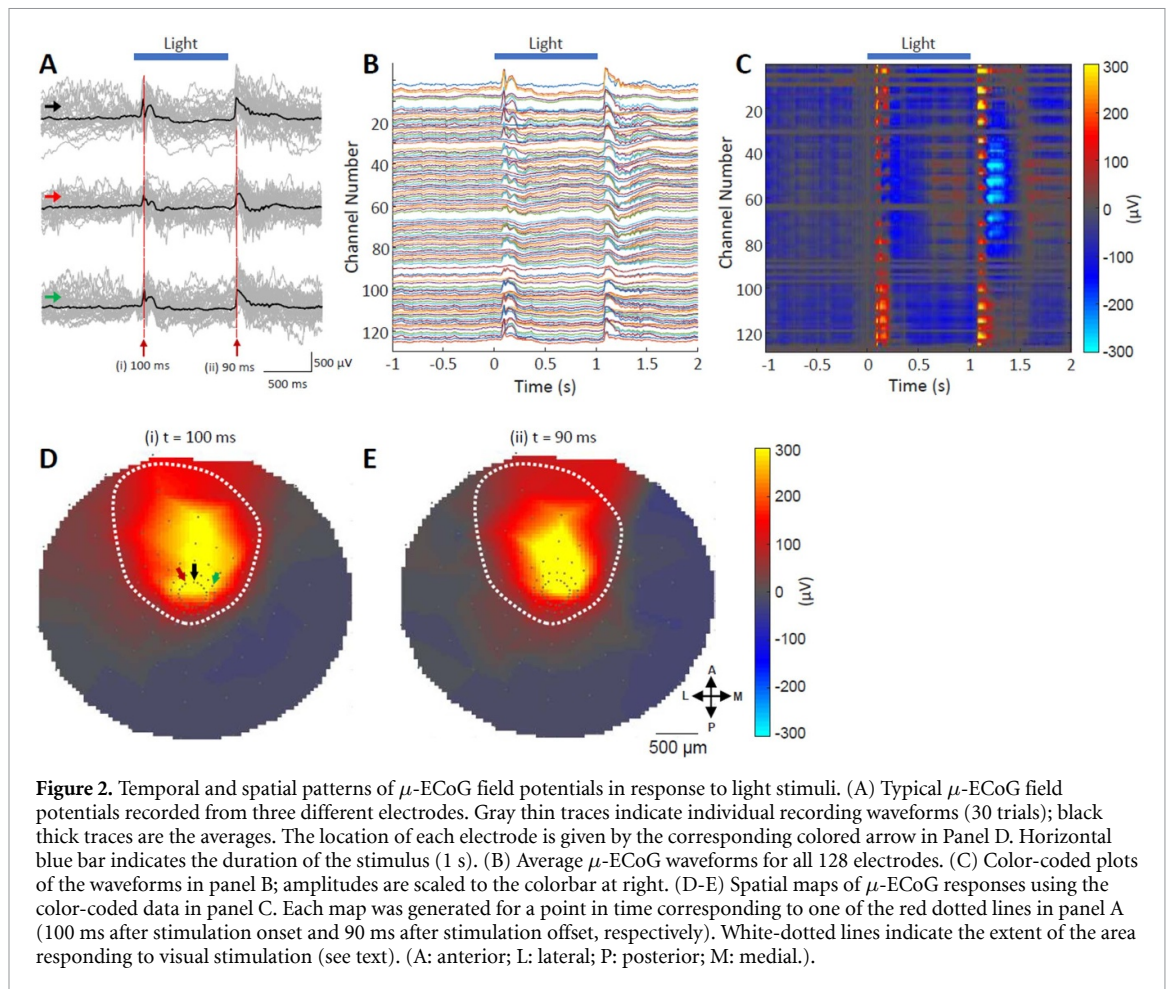
Anesthetized mice were placed into a stereotaxic frame (SR-9 M-HT, Narishige International USA, Inc. Amityville, NY, USA) for the craniotomy as well

as all subsequent testing. A heating blanket on the floor of the frame was used to maintain body temperature at 37.5  $^\circ\text{C}$ . Ear bars were positioned into the auditory canals; a midline incision was made to the scalp; and the skin flaps were retracted to expose the skull. The craniotomy was performed to the area of 4.5 mm x 4.5 mm overlying the primary visual cortex (V1) of the left hemisphere. The exposed cortex was rinsed with phosphate-buffered saline to clear any residual debris on the surface of dura before the recording electrode array was positioned. Before positioning the recording array on the V1, a thin rod (diameter: 125  $\mu\text{m}$ ) with a blunt tip was attached to a micromanipulator (SMM-100, Narishige International USA, Inc. Amityville, NY, USA); and the tip of the rod was positioned on the V1 (anterior-posterior (AP): –3.8 mm, medial-lateral (ML): –2.5 mm ~ –3.0 mm) by a stereotaxic coordinate (Franklin and Paxinos 1997). Subsequently, the recording array was placed over the exposed V1; and the central hole of the array was precisely adjusted under the microscope so that it could be positioned underneath the tip of the rod which was located on top of the V1 area. Once the recording array was positioned on the V1, impedances of electrodes of the array were measured to confirm the viability of the electrodes; and  $\mu\text{-ECoG}$  signals were recorded using the ORH128 Intan Recording System (Hermiz *et al* 2016). Channels with excessive line noise, had high impedances (>100 k $\Omega$ ) were removed from the analysis.

## 2.4. Electric and magnetic stimulation

Prior to electric and magnetic stimulations, visual stimulations were presented to measure visually-evoked potentials (VEPs) with the recording array (figure 2). The visual stimulation was presented from a monitor (HP ZR22w, Hewlett-Packard, Palo Alto, CA, USA) placed at a distance of 25 cm from the mouse; and the screen was oriented at 45 $^\circ$  to the axis of the body so that it was positioned perpendicular to the right eye of the mouse. The visual stimuli consisted of full-field flashes (1 s) that were generated and controlled by custom software written in LabView (National Instruments, Austin, TX, USA) and MATLAB (MathWorks, Natick, MA, USA). Each stimulus was repeated at least 30 times.

Electric stimulation was presented via a monopolar stimulating electrode (Platinum-Iridium (Pt-Ir); tip diameter: 2–3  $\mu\text{m}$ ; impedance: 10 k $\Omega$ ; PI2PT30.01 A10; Microprobes for Life Science, Gaithersburg, MD, USA). The electrode was mounted on a micromanipulator (SMM-100, Narishige International USA, Inc. Amityville, NY, USA); and inserted into the V1 through the central hole of the recording array (figures 1(C) and (D)). The tip of the electrode was first positioned at a depth of 250  $\mu\text{m}$  from the cortical surface to target cortical neurons in layers 2/3 (L2/3) located in depths of 100–350  $\mu\text{m}$  (Olsen



*et al* 2012, Ryu *et al* 2019). Electric stimuli were controlled by Multi Channel Systems MCS (Reutlingen, Germany) STG2004 hardware and software. Stimulus waveforms consisted of cathodic-first rectangular biphasic pulses with phase duration of 200  $\mu$ s and no inter-phase-interval. One trial of stimulation consisted of 20 pulses at a repetition rate of 200 Hz; and total 20 trials were repeated with an inter-trial-interval of 10 s (figure 1(E)). Stimulation amplitudes ranged from 10  $\mu$ A to 30  $\mu$ A. After recording the  $\mu$ -ECoG responses to electric stimulation of L2/3, the tip of the electrode was adjusted to a depth of 550  $\mu$ m to target neurons in the layer 5 (L5) located in depths of 450–650  $\mu$ m; and the electric stimulation was repeated.

Magnetic stimulation was presented via a custom micro-coil (figure 1(F)) that was inserted through the hole of the array and positioned in the V1. Similar to the previous study (Lee *et al* 2016), the coil was constructed by carefully bending a 25  $\mu$ m-diameter Pt-Ir wire with 4- $\mu$ m-thick polytetrafluoroethylene insulation (A-M Systems, Sequim, WA, USA); and the resulting structure had a cross-sectional area of  $100 \times 33 \mu\text{m}$ . The length of the coil was 30 mm; and the direct current (DC) resistance of the coil was 24.2  $\Omega$ . The coil had two terminals that were connected with a 1000-W audio amplifier (PB717X, Pyramid

Inc. Brooklyn, NY, USA) via lead wires. The lead wires had a DC resistance of 1.2  $\Omega$ , and therefore the DC resistance of the entire structure was 25.4  $\Omega$ . Stimulus waveforms were controlled by a function generator (AFG3021B, Tektronix Inc. Beaverton, OR, USA) and amplified by the audio amplifier with a gain of 8 V/V and a bandwidth of 70 kHz. The audio amplifier was powered by a battery (LC-R1233P, Panasonic Corp., Newark, NJ, USA). Stimulation pulses consisted of a single full-period 1-kHz sinusoid waveform with a  $-90^\circ$  phase shift (figures 1(E) and (G)). The amplitude of sinusoids from the function generator ranged from 0 V to 2.5 V. The output of the amplifier for sinusoids was 0 V to 20 V. Similar to the electric stimulation above, one trial of stimulation (figures 1(E) and (G)) consisted of 20 pulses at the repetition rate of 200 Hz; and total 20 trials were repeated with the inter-trial-interval of 10 s. The tip of the coil was located at the depths of 250  $\mu$ m and 550  $\mu$ m to target the neurons in L2/3 and L5, respectively.

In our study, we typically ran experiments with the microelectrode prior to running experiments with the micro-coil because the tip of the electrode (e.g. 2–3  $\mu$ m in diameter) was considerably smaller than that of the micro-coil (e.g.  $100 \times 33 \mu\text{m}$ ), and therefore, we expected much less tissue damage from

insertion of the electrode compared to that caused by subsequent insertion of the micro-coil. In some experiments, we inserted the micro-coil only and obtained results that were almost identical to those that occurred following electrode insertion ( $n = 11$  mice) (e.g. threshold and spatial extent of activation). This supports our hypothesis above, e.g. the insertion of the electrode did not cause tissue damage above and beyond that caused subsequently by the coil, and therefore did not affect the results obtained with the micro-coil. The stimulation frequency was also fixed at 200 Hz for both electric and magnetic stimulation, a frequency used commonly in cortical visual prostheses (Beauchamp *et al* 2020).

### 2.5. Temperature measurement

Since the current level used for the magnetic stimulation in this study is relatively higher than that for electric stimulation, we conducted experiments to verify that the activation during the magnetic stimulation was not the result of thermal activation of neurons. Therefore, we monitored the change in temperature during experiments with magnetic stimulation by measuring temperature of the surface of the coil. This was done in D.I. water at room temperature (typically 21.6 °C) with the probe in direct contact with the coil tip. Similar to the physiological experiments, a train of 20 pulses, each with a period of 1-kHz (half sine waveform), was delivered at a repetition rate of 200 Hz. The interval between presentation was 1 s and the temperature was reported immediately after the completion of ten presentations.

### 2.6. Data analysis

Data was acquired at 30 kHz and filtered by default Intan setting with cutoffs 1 Hz to 7.5 kHz and using OpenEphys acquisition graphic-user interface software (Hermiz *et al* 2016) (<http://www.open-ephys.org/>), with the impedance tests of the electrodes during the experiments carried out using the Intan RHD2000 software from Intan Technologies (Los Angeles, CA). Data was extracted and processed using MATLAB (Mathworks, Natick, MA).

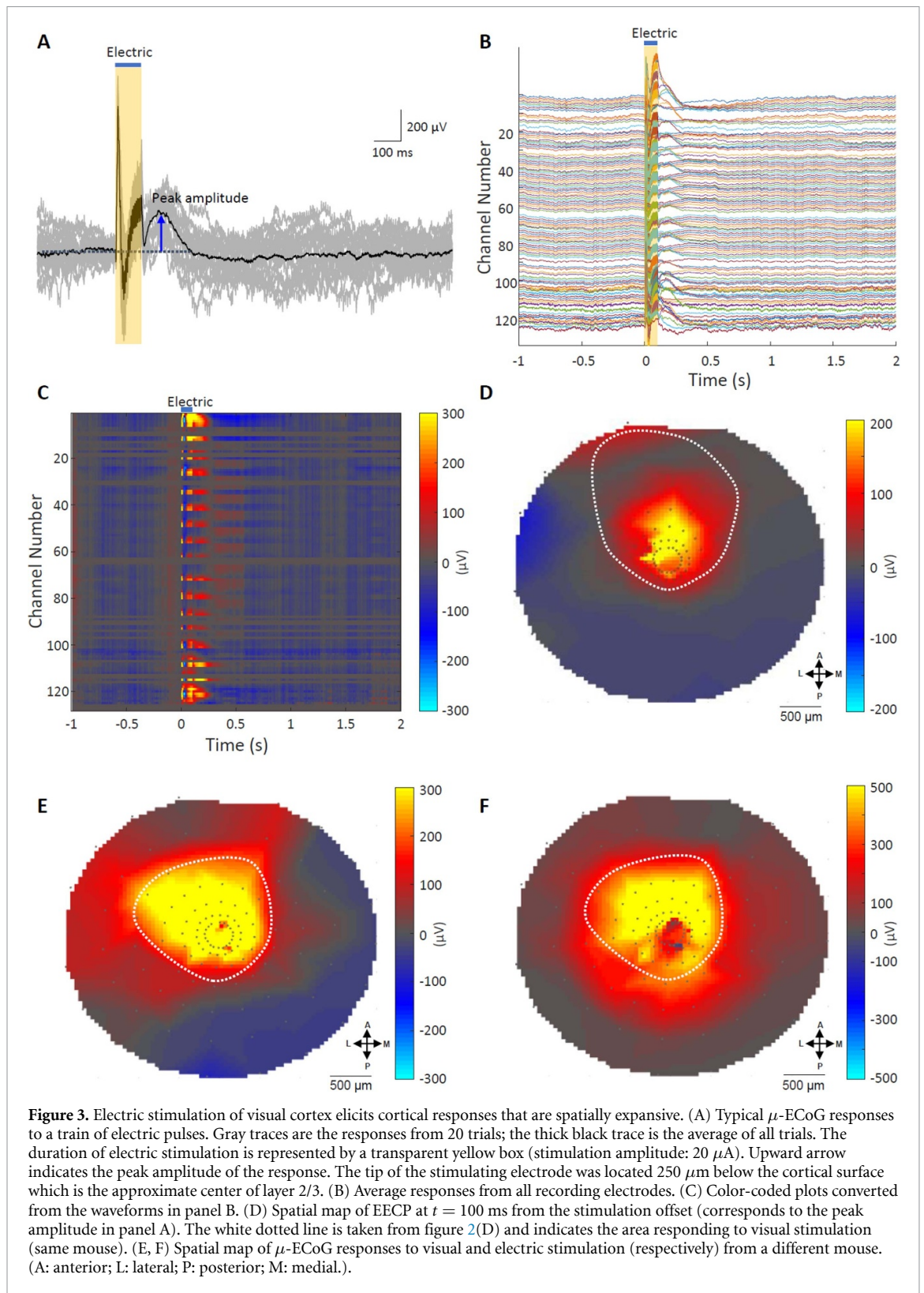
All voltage data used in this study were local field potentials (LFPs), and those were derived from raw data. The LFP data were decimated to 1000 Hz and demeaned. Line noise (60 Hz, 120 Hz, 180 Hz) was removed by subtracting band-passed signals from the raw signal. Channels with excessive line noise or without clear neural signal were removed from the analysis. The evoked  $\mu$ -ECoG potential responding to stimulation was analyzed by extracting epochs from 1 s before stimulation onset to 2 s after offset. The extracted epochs for all channels were averaged as shown in figures 2(A) and (B) and then converted into color-coded plots (figure 2(C)) according to the scale bar on the right. After that, color-coded spatial maps at each time point were constructed by mapping

the color data to the circular array; and colors between electrodes were interpolated (figures 2(D) and 2(E)).

To investigate spatiotemporal patterns of cortical responses, we measured the peak amplitudes of  $\mu$ -ECoG responses to electric and magnetic stimulation versus distance from the stimulation site (the center of the recording array). Electric stimulation produced typical  $\mu$ -ECoG responses that consist of positive voltage deflections (figure 3(A)), and we measured the peak amplitudes of the positive waveforms that occurred during the time period of 1 s after completion of the stimulation. To quantitatively detect and compare the  $\mu$ -ECoG responses to electric stimulation across different stimulating conditions, we developed criteria to determine whether each response was supra-threshold. This required some care however since baseline noise levels varied substantially between channels, i.e. it was not possible to set a uniform value for threshold across all channels. Instead, we normalized the signal from each channel independently by measuring the baseline noise level, defined as the mean background signal across the 900 ms time period preceding each stimulus, and then set the threshold level relative to this baseline (defined as three standard deviations (3xSD) of the background noise level above the mean) (figure 5(A)). This 3xSD is related to a confidence interval 99.7% and also used to detect evoked LFPs with similar shapes as those reported by Basu *et al* (2019). The blue and red horizontal lines in each panel of figure 5(A) represent the 3xSD level (above mean baseline) and serve as threshold for that response (blue and red correspond to stimulation of L2/3 and L5, respectively).

Unlike the electric stimulation, magnetic stimulation produced  $\mu$ -ECoG signals that consist of negative waveforms (figures 6(A) and (B)). In order to determine whether the negative waveforms are indeed neural responses, we recorded the signals after euthanasia of the animals by injection of the anesthetic overdose (see 'Animal preparation') without moving the inserted micro-coil. We found that the negative waveforms remained after the euthanasia and the most of the signals seemed stimulation artifacts (cf. figures 6(A) and 6(B)). However, we also noted that there were small differences in signal size and shape before and after the euthanasia. Therefore, the signals from a live animal are subtracted by those of euthanized animal (figure 6(C)), and the positive waveforms remained. We assumed that these positive waveforms contain cortical responses; and the peak amplitudes of those waveforms from each channel were measured during the time period of 1 s after the stimulation onset. Like the criteria used for electric stimulation, three standard deviations (3xSD) of the background noise level above the mean served as the threshold to determine whether each response was supra-threshold.

For statistical analysis, the Student (independent sample)  $t$ -test was used,  $p < 0.05$  was considered as



significant. In figures presenting the median of data, error bars denote the standard error of the mean.

### 3. Results

A 128-channel PEDOT:PSS recording array was used to obtain epidural  $\mu$ -ECoG signals from mouse visual

cortex in response to light, electric and magnetic stimuli. The high channel count and wide spatial coverage provided by the array allowed ECoG patterns to be studied in detail for different parameters of stimulation within each modality, as well as across modalities. The results below are based on experiments in 11 mice.

### 3.1. VEPs from light are spatially broad

To identify the location as well as the spatial extent of V1, we measured VEPs with the  $\mu$ -ECoG recording array. The  $\mu$ -ECoG array was first positioned over mouse V1 using previously described stereotaxic coordinates (Franklin and Paxinos 1997) (figures 1(C) and (D)). Once the array was in place, full-field light stimuli were presented (Materials and Methods); gray traces are the responses to individual presentations ( $n = 30$ ), and the average response is shown in black (figure 2(A)).  $\mu$ -ECoG signals typically exhibited positive peaks at latencies of 100 ms following stimulation onset along with an additional positive peak approximately 90 ms after stimulation offset (red-dotted lines). Overlay of the average response from all 128 channels (figure 2(B)) revealed similarity in timing across many responding channels. Averaged responses were converted to scaled colors (figure 2(C)) so that spatial maps could be constructed (figure 2(D), the three colored arrows correspond to the three traces of figure 2(A)). The response patterns of each spatial map varied considerably as the response progressed but the location of the biggest responses were consistent in their location (the maps in figures 2(D) and (E) correspond to the two peak response latencies in figure 2(A)). Consistent with previous reports (Polack and Contreras 2012, Murakami *et al* 2017), visually evoked responses were spatially broad, typically extending 1–2 mm across the cortex. If the VEP extended beyond the edge of the array during initial measurements, the array was re-centered and light responses re-captured; centering helped to ensure that responses to electric or magnetic stimulation delivered through the central hole of the array were confined to visually responsive cortex and were within the limits of the array in subsequent experiments. We did not perform additional analysis of the VEPs.

### 3.2. Spatiotemporal pattern of electrically-evoked $\mu$ -ECoG field potentials was shaped by stimulation amplitude and location

After measurements of VEPs were completed, a stimulating electrode was inserted through the central hole of the array and penetrated into the cortex (figure 1(E), top right); the depth of penetration was controlled by a micromanipulator (Materials and Methods). Stimulation typically consisted of 20 biphasic pulses via monopolar stimulation; the resulting responses are referred to as electrically-evoked cortical potentials (EECPs). A typical EECP response for insertion of the electrode tip to the approximate center of L2/3 ( $\sim 250 \mu\text{m}$ ) (Olsen *et al* 2012, Ryu *et al* 2019), is shown in figure 3(A). A large electrical artifact resulted from the stimulus but it was confined to the 100 ms time period during which the stimulus was delivered (yellow shaded area); we did not systematically analyze the properties of the artifact but casual

observation revealed it to be multiphasic with variability across different parameters of stimulation and/or different recording locations. We did not try to isolate or identify neural responses during this time period.

After completion of the stimulus, many channels exhibited a sustained positive-going response that peaked  $\sim 100$  ms after stimulus offset (blue arrow); the kinetics of the response were similar across many channels (figure 3(B)). Analogous to the approach with VEPs, each response was color-coded (figure 3(C)) so that the spatial profile across the cortical surface could be mapped (figure 3(D)). The spatial map in figure 3(D) corresponds to a latency of 100 ms from stimulation offset (the time at which response amplitude was maximal) and reveals strong activation that extends well beyond the stimulation site (the center of the array), e.g. the bright yellow area extended up to the fifth ring of recording electrodes, approximately  $1047 \mu\text{m}$  from the center. Note that EECPs did not spread uniformly and concentrically from the stimulation site but instead, typically activated the same regions of the cortical surface that were activated by light, e.g. the white-dotted line in figure 3(D) is taken from figure 2(D) and corresponds to the area activated by visual stimulation for that mouse. Figures 3(E) and (F) are the visual and electrical responses, respectively, from another mouse and show qualitatively similar responses. The broad and asymmetric spatial activation found here is consistent with the previous work that showed that a single pulse of electric stimulation delivered to V1 activated areas of V1 and V2 without strongly activating other nearby (non-visual) cortical areas, i.e. the areas activated by electric stimulation in V1 reflect the synaptic connections of visual cortex (Fehervari *et al* 2015, Fehervari and Yagi 2016).

EECPs were influenced by the amplitude of stimulation as well as by the layer at which stimulation was delivered (figure 4). In general, stimulation of L5 resulted in responses that were spatially broader than those from stimulation of L2/3, e.g. compare the response to a  $20 \mu\text{A}$  stimulus delivered to L2/3 (figure 4(A), 200 ms) to the same stimulus delivered to L5 (figure 4(C); 200 ms). It was somewhat surprising that spatially broader responses arose from stimulation of the deeper layer, i.e. volume conduction of a given neural signal would be expected to be stronger and broader for stimulation delivered closer to the cortical surface. Nevertheless, this finding is consistent with previous studies which showed that stimulation of L5 produces cortical activity that spreads further in the horizontal directions. (Telfeian and Connors 1998, Hishida *et al* 2011). Given this wide spread of activation, it is likely that some form of active conduction is contributing to the spread of EECPs, at least those from L5. Responses were also sensitive to the amplitude of stimulation with larger amplitudes leading to spatially broader regions of activation, regardless of the stimulation

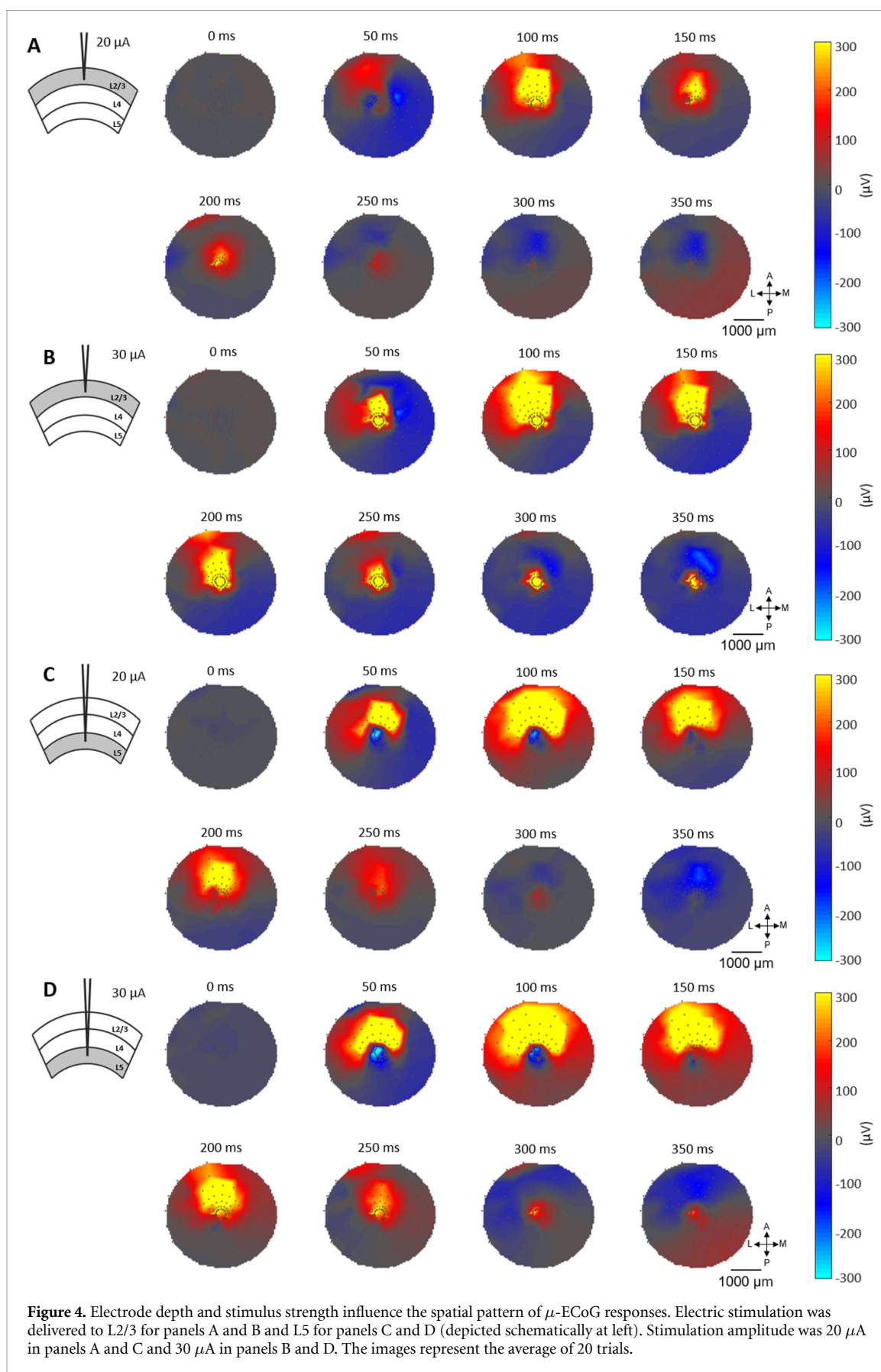


**Figure 4.** Electrode depth and stimulus strength influence the spatial pattern of  $\mu$ -ECoG responses. Electric stimulation was delivered to L2/3 for panels A and B and L5 for panels C and D (depicted schematically at left). Stimulation amplitude was 20  $\mu\text{A}$  in panels A and C and 30  $\mu\text{A}$  in panels B and D. The images represent the average of 20 trials.

layer at which stimulation was delivered, e.g. compare the spatial extent of the responses for corresponding time points in figures 4(A) to (B) and (C) to (D).

To quantitatively compare the spatial extent of EECs across different stimulating conditions, we developed criteria to determine whether each response was supra-threshold (Materials and Methods). Briefly, three standard deviation (3xSD) of the background noise level above the mean of each channel was used as a threshold for the given channel (figure 5(A)). The blue and red horizontal lines in each panel of figure 5(A) represent the 3xSD level (above mean baseline) and serve as threshold for that response (blue and red correspond to stimulation of L2/3 and L5, respectively). The location of the recording electrode is indicated by a red dot in the schematic to the left of each row; distance from the center is listed below. We generated maps to show the location of all responding electrodes (i.e. ones for which peak response exceeded 3xSD, colored white) and non-responding electrodes (gray pixels) (figure 5(B)); the number of activated pixels was then counted to estimate the size of the area activated by electric stimulation. Consistent with the qualitative patterns of figures 3 and 4, the spatial extents of EECs were quite large (figure 5(B)); even for moderate levels of stimulation (20  $\mu$ A), the response extended almost 8 mm<sup>2</sup> (almost the entire extent of the visual cortex). At even higher amplitudes (30  $\mu$ A), the size of the response to L5 stimulation increased slightly while that from L2/3 stimulation decreased somewhat (figure 5(C)).

To examine response strength vs. distance from the site of stimulation it was necessary to determine mean response strength at each distance (Materials and Methods). However because responses were typically not radially symmetric (compare responses above and below the central hole in the panels of figure 4), responses from all electrodes in each ring could not simply be averaged to yield the mean response strength at a given distance. Instead, we averaged only those channels that generated responses >3xSD (figure 5(A)). Response strength vs. distance was calculated for low, medium and high stimulus amplitudes for both L2/3 and L5 stimulation (figure 5(D)). Responses were stronger for L2/3 stimulation, especially at high stimulation levels, but fell off quickly with distance. There was little difference between L2/3 and L5 responses at distances  $\geq 1$  mm.

### 3.3. Responses to magnetic stimulation are spatially confined

Analogous to the experiments with electric stimulation, a micro-coil was inserted into the cortex through the central hole of the array and  $\mu$ -ECoG responses were again measured. Much previous *in vitro* work with micro-coils has shown that the spatial spread of responses to stimulation is more confined vs. that from electrodes (Lee et al 2016, 2019).

This is thought to arise because the spatially asymmetric fields induced from coils are suprathreshold for vertically-oriented pyramidal neurons but not for horizontally-oriented passing axons and thus there is less secondary spread with coils. Here, we sought to understand whether such differences would analogously translate to *in vivo* differences as measured by the  $\mu$ -ECoG signals. Responses were again compared for stimulation of either L2/3 or L5. Figure 6(A) (left panel) shows the responses to individual trials of magnetic stimulation (gray lines) from a single recording electrode within the innermost ring of the array; the thick black line is the average of the response of all individual trials ( $n = 20$ ). In contrast to the positive-going responses to electric stimulation (figure 3(A)), the response to magnetic stimulation consisted of a steep, negative deflection; the onset of the negative deflection started while the stimulus was ongoing and persisted until briefly after termination of the stimulus; the return to baseline was more gradual. Overlay of all responses (figure 6(A), middle panel) revealed similarities across many recording locations although a smaller number of channels responded to magnetic stimulation (vs. electric stimulation). The sparseness of responses can perhaps be better seen in the color-coded response overlay (figure 6(A), right panel, compare to that from electric stimulation). Mapping the responses to magnetic stimulation revealed that responses were largely confined to only those electrodes close to the coil, typically those within the second or third ring (corresponding to distances of 275–448  $\mu$ m from the center) (figure 6(A), left, inset). The narrow spread of activation with magnetic stimulation is in stark contrast to the spatially broad responses arising from electric stimulation.

The negative going responses to magnetic stimulation were somewhat surprising given the responses to electric stimulation were positive (figures 3(A) and (B)). We considered the possibility that the electrical artifact arising from the magnetic stimulus was distorting response polarity and tried to estimate the size and shape of the artifact by comparing the responses measured in living animals to responses obtained after animals were euthanized (Materials and Methods). As shown in figure 6(B), the temporal and spatial pattern of the signals recorded from the euthanized animal were largely similar to those recorded from the live animal (overlay of the two signals is shown in figure 6(C), top) although interestingly, subtraction of the signal in the euthanized animal (presumably the stimulus artifact) from that in the living animal (artifact plus neuronal response) resulted in a positive going response (figure 6(C), bottom), now consistent with the polarity of the responses to electric stimulation. We refer to the signals obtained after the subtraction of the euthanized response from the living response as the magnetically-evoked cortical potentials (MECPs) and

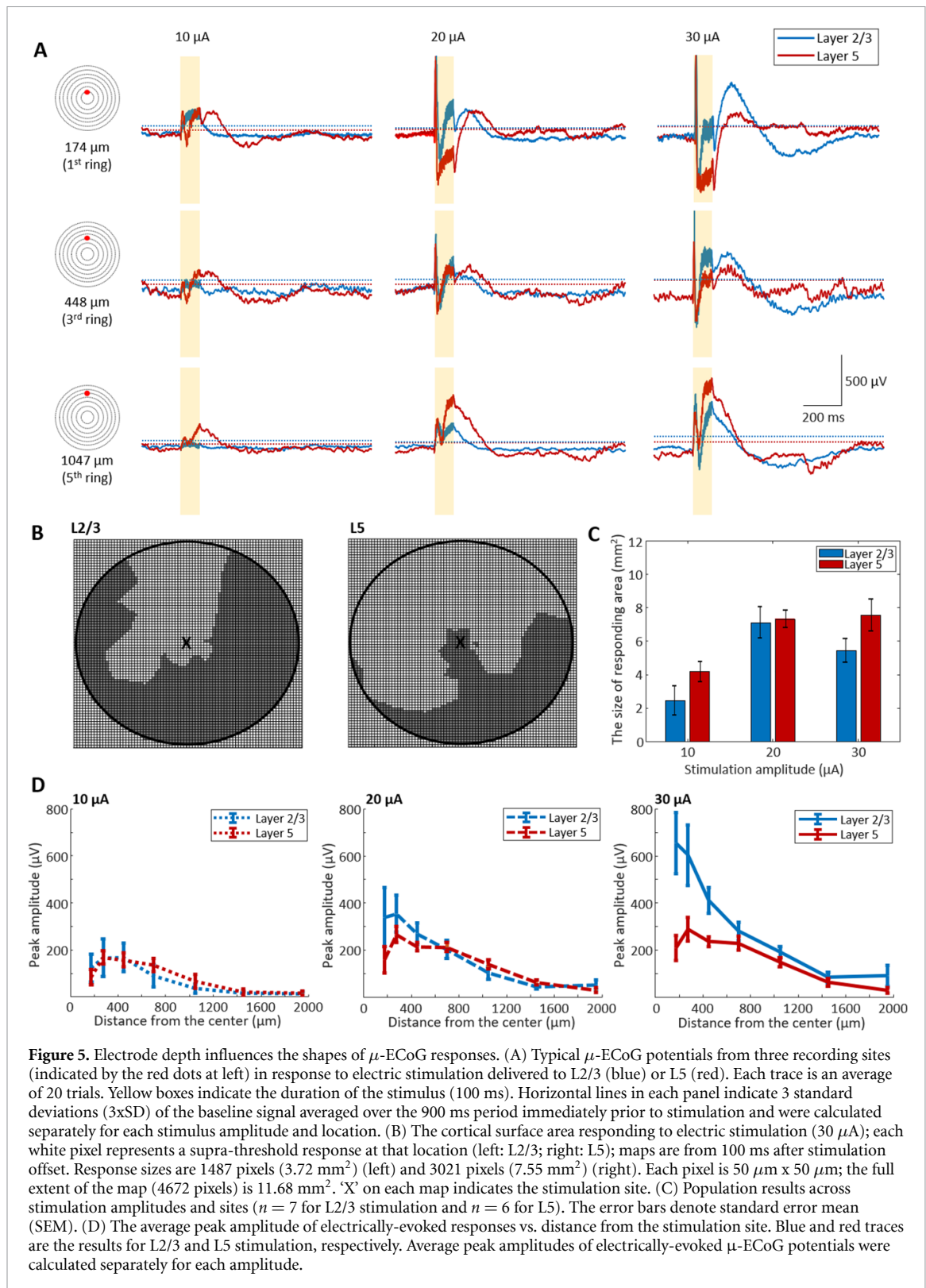
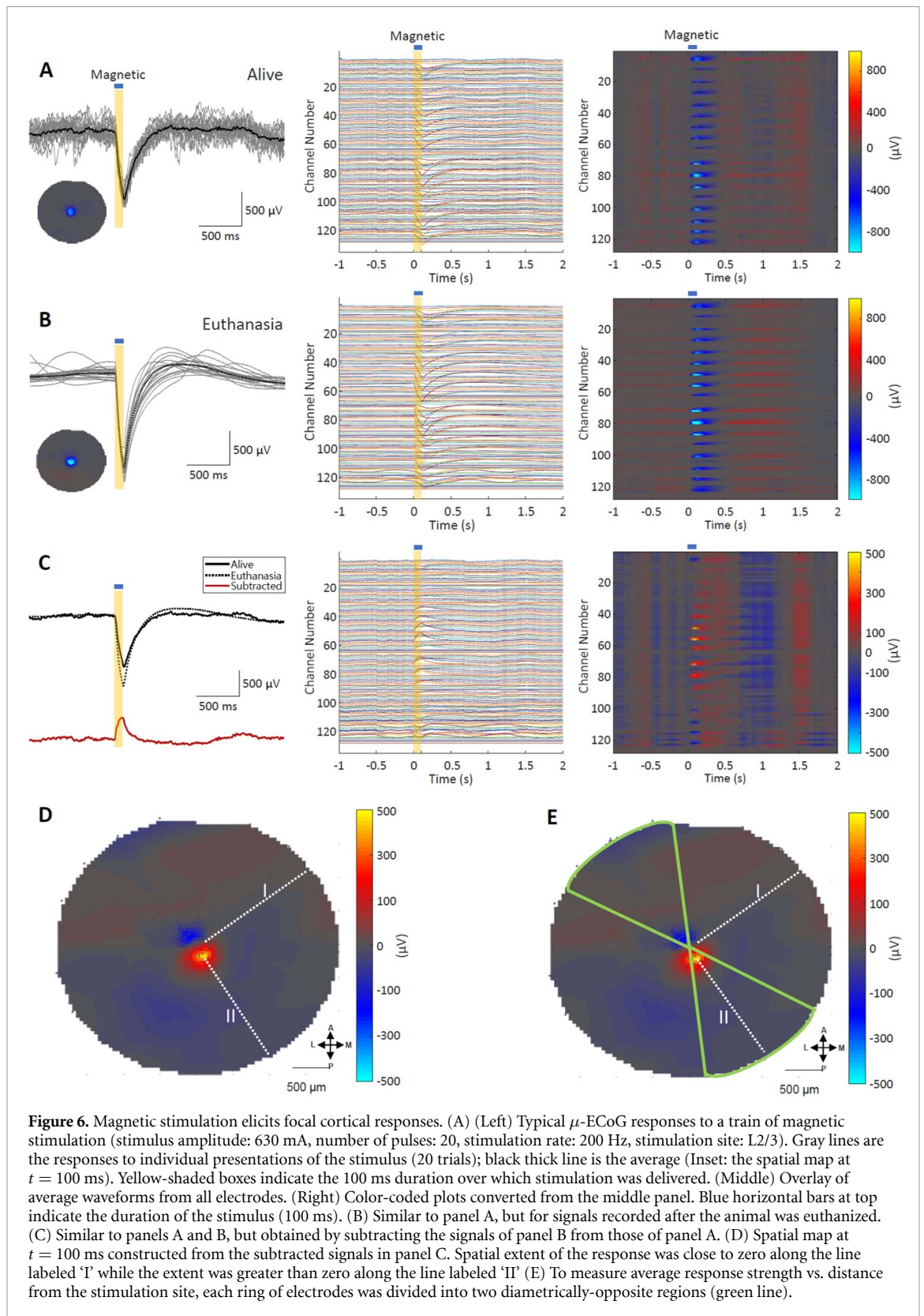


**Figure 5.** Electrode depth influences the shapes of  $\mu$ -ECoG responses. (A) Typical  $\mu$ -ECoG potentials from three recording sites (indicated by the red dots at left) in response to electric stimulation delivered to L2/3 (blue) or L5 (red). Each trace is an average of 20 trials. Yellow boxes indicate the duration of the stimulus (100 ms). Horizontal lines in each panel indicate 3 standard deviations ( $3\times\text{SD}$ ) of the baseline signal averaged over the 900 ms period immediately prior to stimulation and were calculated separately for each stimulus amplitude and location. (B) The cortical surface area responding to electric stimulation ( $30\ \mu\text{A}$ ); each white pixel represents a supra-threshold response at that location (left: L2/3; right: L5); maps are from 100 ms after stimulation offset. Response sizes are 1487 pixels ( $3.72\ \text{mm}^2$ ) (left) and 3021 pixels ( $7.55\ \text{mm}^2$ ) (right). Each pixel is  $50\ \mu\text{m} \times 50\ \mu\text{m}$ ; the full extent of the map (4672 pixels) is  $11.68\ \text{mm}^2$ . 'X' on each map indicates the stimulation site. (C) Population results across stimulation amplitudes and sites ( $n = 7$  for L2/3 stimulation and  $n = 6$  for L5). The error bars denote standard error mean (SEM). (D) The average peak amplitude of electrically-evoked responses vs. distance from the stimulation site. Blue and red traces are the results for L2/3 and L5 stimulation, respectively. Average peak amplitudes of electrically-evoked  $\mu$ -ECoG potentials were calculated separately for each amplitude.

use this approach for all subsequent analyses. The middle and right panels of figure 6(C) show the MECPs from all electrodes and confirmed that many responses were now positive, e.g. the color-coded signals contained warm colors in the time period following stimulation (figure 6(C), right). The spatial map (figure 6(D)) confirmed that responses were narrowly confined around the site of stimulation, e.g. within

the first two rings of electrodes (figure 6(D)). The MECP also revealed a spatially distinct region of negative responses (bright blue portion of the map) directly adjacent to the strong positive responses (bright yellow); a qualitatively similar result was observed in three of the four animals for which magnetic stimulation was delivered to L2/3. We did not attempt to identify the factors contributing to the biphasic



response pattern although it is possible that differences in the polarity of the induced electric field on the two sides of the coil mediate the different polarities. Biphasic responses were not observed for stimulation of L5 ( $n = 4/4$ ). Despite being narrowly confined, MECP magnitudes generally increased with increasing stimulation strength (compare responses

in figure 7(B) vs. those in 7(A)). In further contrast to the responses to electric stimulation, MECP responses were stronger for stimulation of L2/3; but the responses to stimulation of L5 were barely detectable for lower amplitude stimuli (figure 7(C)).

Similar to the responses to electric stimulation, the responses to magnetic stimulation were

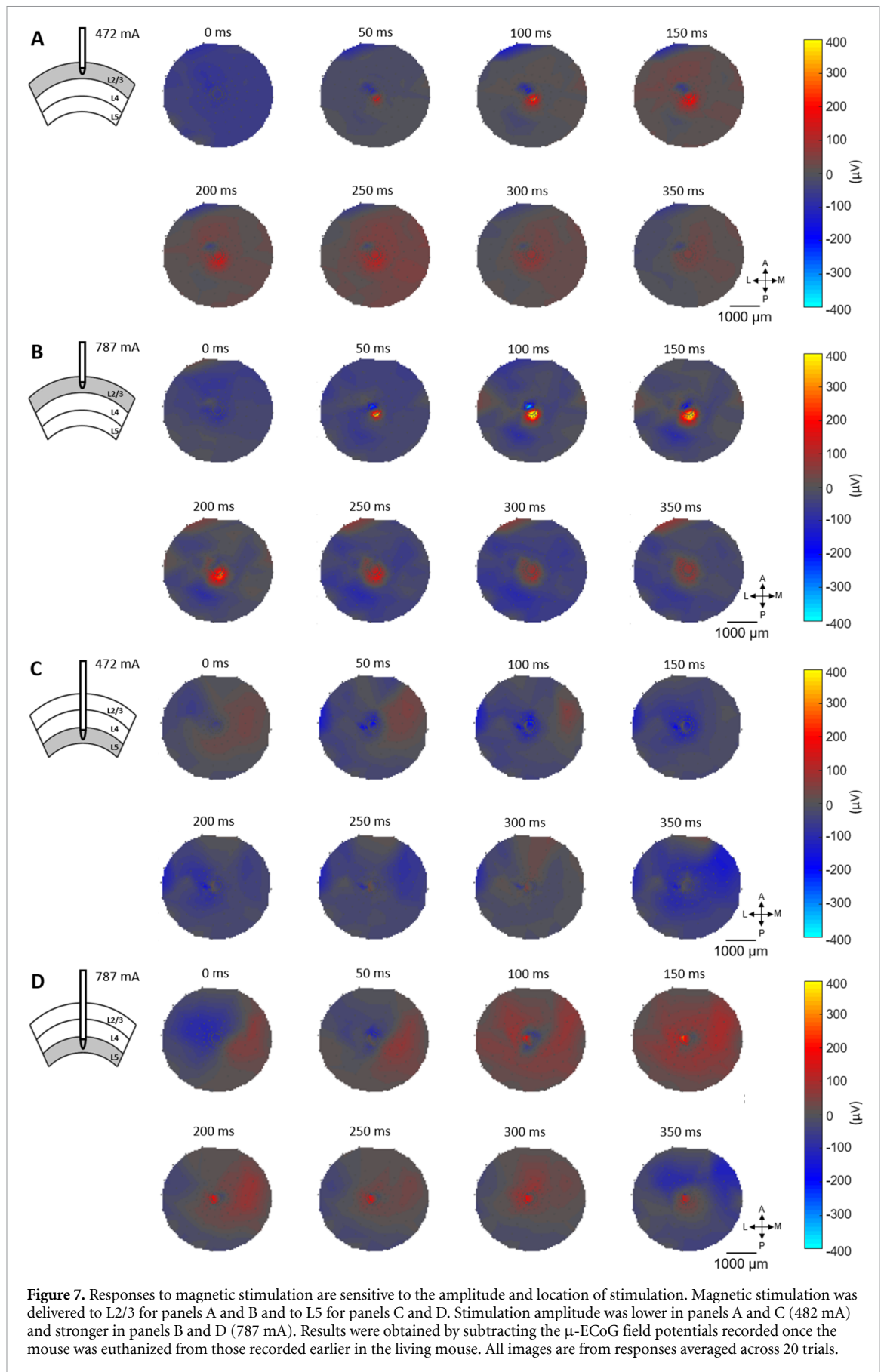
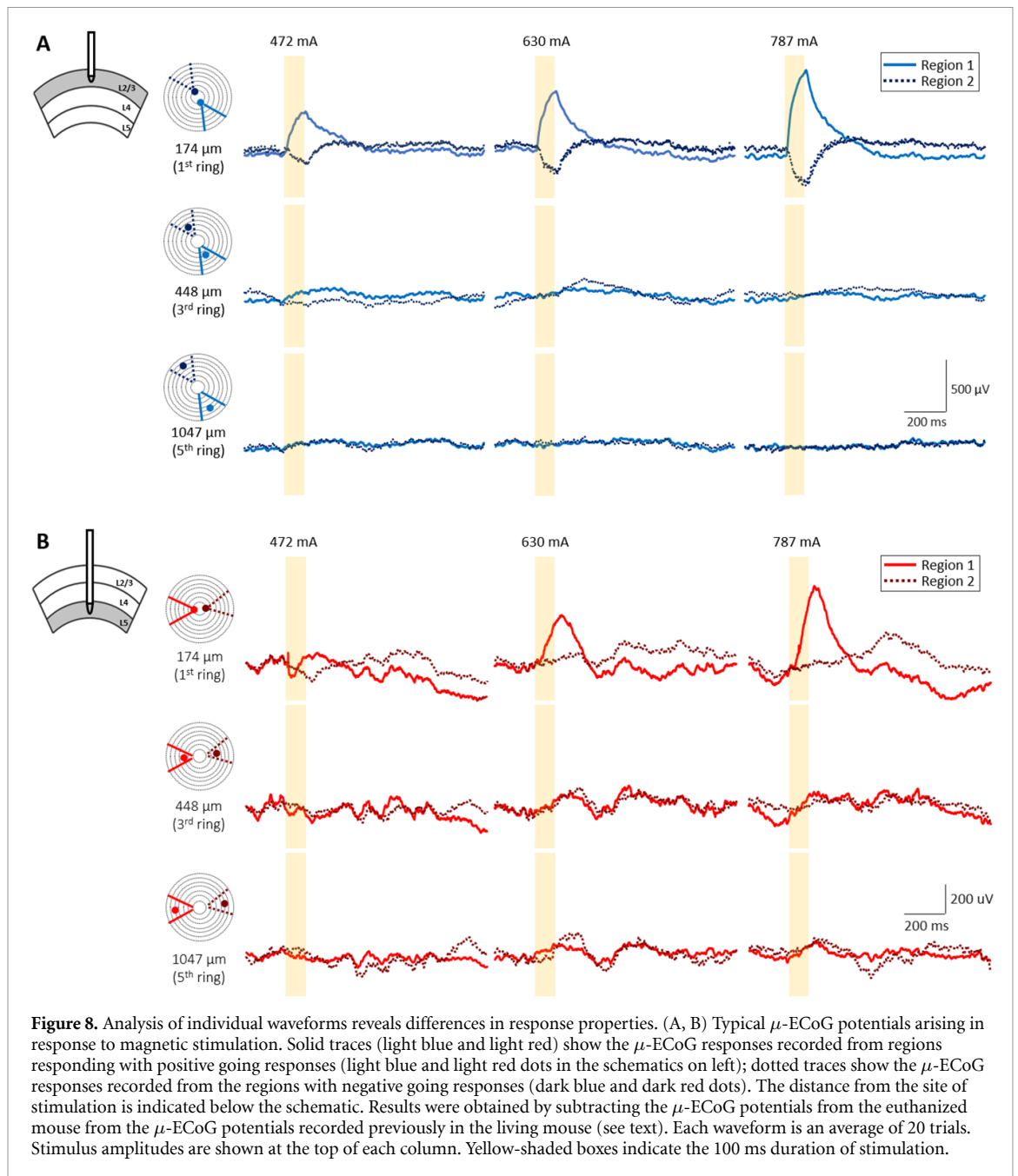


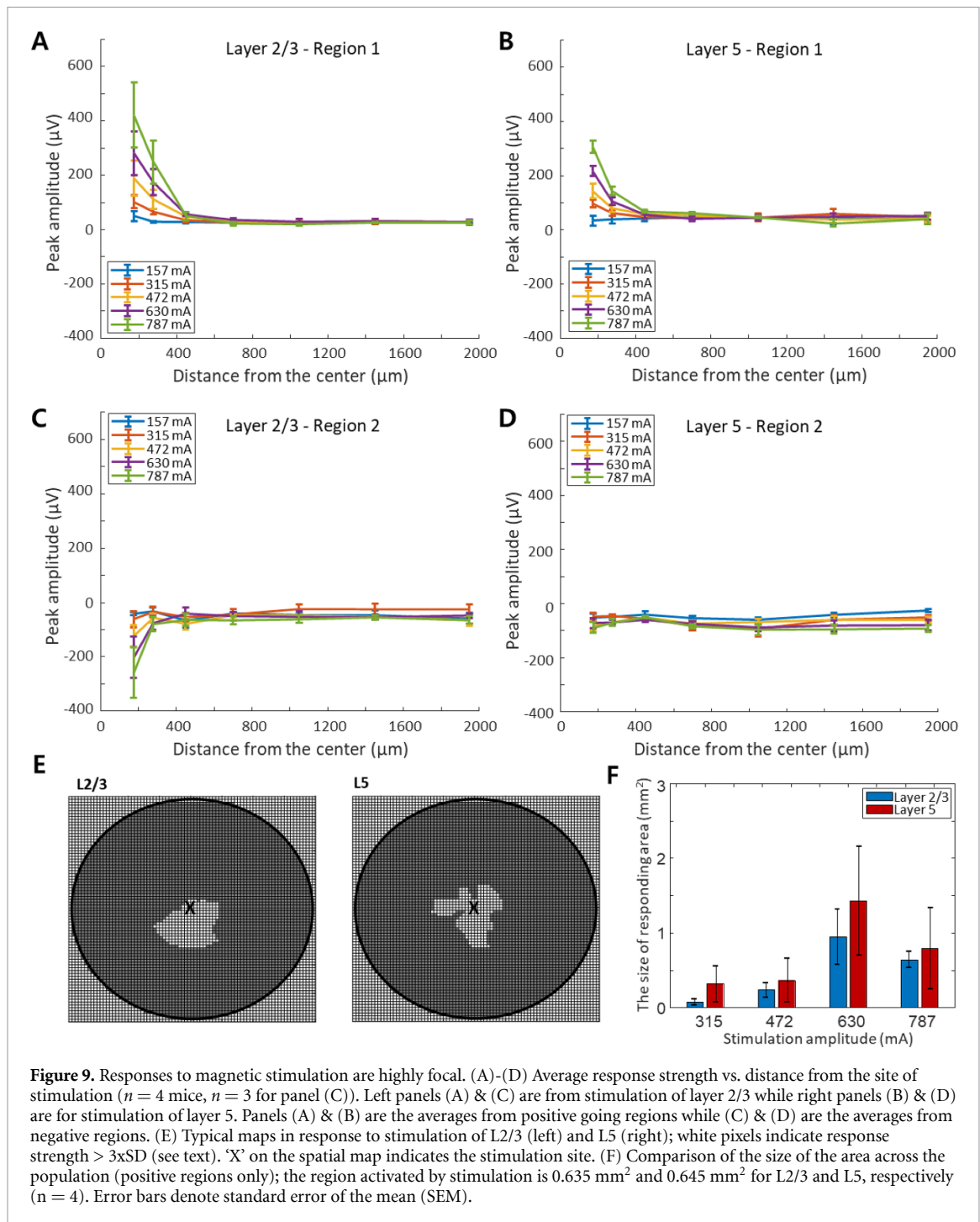
**Figure 7.** Responses to magnetic stimulation are sensitive to the amplitude and location of stimulation. Magnetic stimulation was delivered to L2/3 for panels A and B and to L5 for panels C and D. Stimulation amplitude was lower in panels A and C (482 mA) and stronger in panels B and D (787 mA). Results were obtained by subtracting the  $\mu$ -ECoG field potentials recorded once the mouse was euthanized from those recorded earlier in the living mouse. All images are from responses averaged across 20 trials.



not circularly symmetric e.g. the response along the white dotted line labeled I in figure 6(D) is quite weak while much stronger along the line labelled II. As such, simple averaging of responses at a fixed radial distance would not yield an accurate representation of response strength. To address this, each ring of recording electrodes was divided into two diametrically-opposite regions and response strength was calculated separately in each (the two regions are indicated by solid green lines in figure 6(E)).

In this manner, the spatial spread of MECPs was quantified for different stimulus strengths and different locations of the coil (figure 8). Typical responses are shown in figures 8(A) and (B) for stimulation of L2/3 and L5, respectively. Successive rows in each panel correspond to increasing distance from the stimulation site (see schematics to the left

of each row) and successive columns correspond to increasing stimulation strength. The response within the approximate center of the region with the positive going response is indicated by solid traces (light blue and light red) and is overlaid with a response from an electrode in the center of the negative going region (dark blue dotted traces). Note that only positive going responses arose in response to stimulation of L5 (figure 8(B)). Responses from both stimulus locations were sensitive to the strength of the stimulus (figures 9(A)–(D)) with a rapid decline in response strength with distance. Response strengths were near zero for recording electrodes in the third ring (distances of 448  $\mu$ m), even for the strongest amplitudes tested. Note that stronger levels of stimulation were needed to elicit responses from L5, e.g. the lowest amplitude tested (472 mA) did not elicit



MECPs when delivered from L5 but did from L2/3 (figure 8(A) vs. (B), the top row and left traces in each figure). The size of the area responding to magnetic stimulation was estimated using the same approach for electric stimulation (counting the number of activated pixels, i.e.  $> 3\text{xSD}$ ). Typical responses are shown in figure 9(E). All responses remained focal, e.g.  $< 2 \text{ mm}^2$ , and most were confined to  $< 1 \text{ mm}^2$  (figure 9(F)).

#### 4. Discussion

We stimulated the visual cortex of anesthetized mice with an implanted micro-coil or a micro-electrode

and compared cortical responses (i.e. ECoG) between the two. Use of a custom 128-channel recording array (Paulk *et al* 2019, Ganji *et al* 2019) positioned on the cortical surface provided dense coverage of the region surrounding the stimulation site and also enabled the full spatial extent of responses to be captured as well. Relatively large regions of the cortical surface were activated in response to stimulation from micro-electrodes, even at relatively low amplitudes, while activation from coils was much more confined, often limited to a single cortical column. These results are highly consistent with previous *in vitro* studies in mouse brain slices widespread activation to stimulation from an electrode and narrow activation

in response to stimulation from the micro-coil (Lee *et al* 2016, 2019) and thus suggest that the spread of activity on the cortical surface largely reflects the spread of activity elicited in the region immediately around the electrode (or coil) tip. The ability of micro-coils to confine activation raises the possibility that visual acuity could be enhanced using a coil-based cortical visual prosthesis, although further technological development will be necessary before such an approach can be implemented (see below).

#### 4.1. Spatial spread of EECF by activation of passing axon fibers

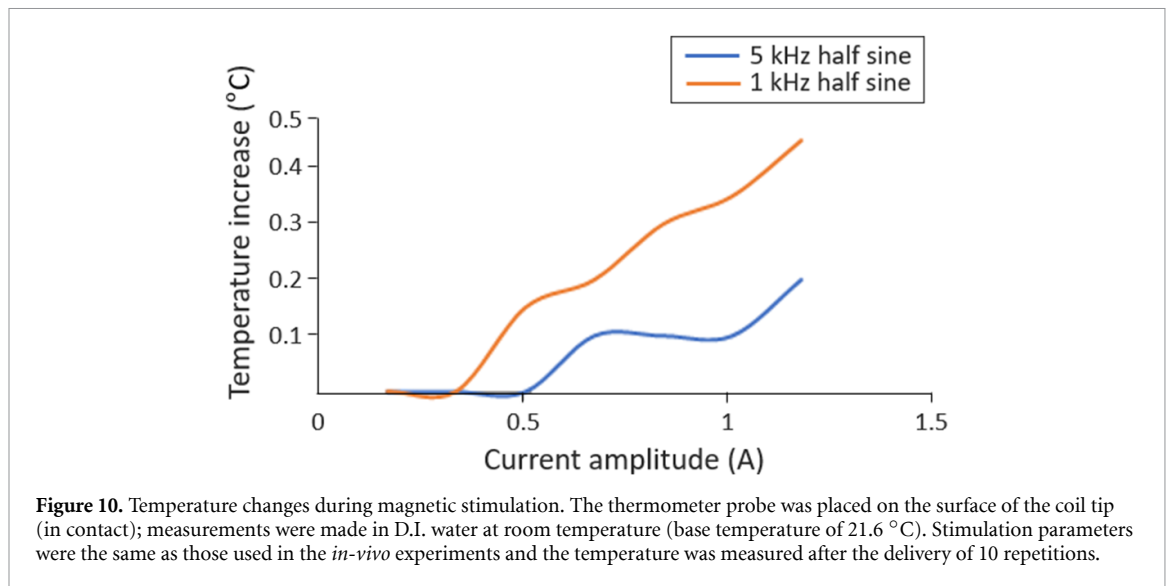
Consistent with previous studies using brain slices, the cortical surface area activated by electric stimulation *in vivo* was also spatially extensive. Peak responses extended  $\sim 2$  mm from the site of stimulation and covered  $\sim 8$  mm<sup>2</sup> of cortical surface area (figures 5(B)–(D)), approximately the full extent of visual cortex. The spread of activation expanded when stimulus strength was increased from low- (10  $\mu$ A) to mid-levels (20  $\mu$ A) but did not expand further when stimulation was increased to 30  $\mu$ A (the maximum levels tested here) (figure 5(C)). These findings are generally consistent with earlier studies of electric stimulation in mouse visual cortex (Hishida *et al* 2011) although many of the specific methodological details differ across studies. For example, Fehervari and Yagi (2016) stimulated with a high-impedance glass electrode and used a single, high-amplitude pulse (50  $\mu$ A) while we used lower impedance electrodes (10 k ohm), a train of pulses (20 pulses delivered at 200 pulses/second) and lower stimulus amplitudes (10–30  $\mu$ A). Further, they used voltage-sensitive dye to assess the spread of activation and thus the signal they captured largely reflects the activity of L2/3 pyramidal neurons (the dye is not thought to penetrate to deeper layers) while the ECoG signals measured here are thought to reflect broader activity from superficial layers and may also reflect propagated activity from deeper layers as well. In addition, the responses they characterized (to a single pulse) arose within a few tens of milliseconds of the stimulus while the responses we studied (to a train of pulses) peaked  $\sim 100$  ms after the termination of stimulation ( $\sim 200$  ms after stimulation onset). The longer latency responses captured here open the possibility that a portion of the response we measured arises from intra-cortical feedback signals (Fehervari *et al* 2015) although the similarity in spread to earlier work (using shorter-latency responses) suggests that if feedback is in fact contributing to our response, it does not expand the region of activation beyond that which arises without feedback. Further, the similarity between studies also suggests that whatever the mechanism(s) underlying the spread of activation, it is triggered by a relatively wide range of stimulus conditions. Studies in non-human primates have reported an analogously large spread in response to

electric stimulation of V1 with activation typically extending to extra-striate cortical regions (Tolias *et al* 2005, Oz *et al* 2020).

It is almost certain that the extensive spread arising from electric stimulation of V1 results from the activation of horizontal fibers (axons) that relay the neural signal from V1 to higher visual centers (Fehervari *et al* 2015). This is consistent with much previous work showing that axons have high sensitivity to electric stimulation (Stoney *et al* 1968, Tehovnik *et al* 2006, Histed *et al* 2009) and are thus likely to be the primary target in response to stimulation from the micro-electrodes used here. Additional support for the activation of axons also comes from the work of Histed *et al* (2009) who used calcium fluorescence changes to measure the simultaneous responses of many L2/3 pyramidal neurons surrounding the stimulating electrode. They found that activation was sparse and distributed around the site of stimulation, instead of uniformly concentrated around the electrode tip, i.e. the pattern was consistent with the activation of axons projecting through the region surrounding the electrode (Histed *et al* 2009). Earlier studies of cortical activation found that the region of activation was proportional to the strength of the stimulus as well as the electrical properties of the surrounding neural tissue with the region of activation typically extending a few hundred microns from the electrode tip (Stoney *et al* 1968). The fact that we (and others) found that activation extends one or more millimeters from the tip adds additional support to the notion that activation of axonal fibers contributes to the spread (with electric stimulation).

#### 4.2. Spatially confined cortical activation by magnetic stimulation

Also consistent with previous findings from *in vitro* studies (Lee *et al* 2016, 2019), we found here that the neural activity arising from micro-coils *in vivo* is much more spatially confined than that from micro-electrodes (figure 6(D)). For example, the spread of MECFs was limited to  $\sim 300$   $\mu$ m from the site of stimulation (figures 9(A) and (B)), much less than  $\sim 2$  mm spread from micro-electrodes (figure 5(D)). Analogously, the size of the activated area with coils was  $\sim 1$  mm<sup>2</sup>, much smaller than the  $\sim 8$  mm<sup>2</sup> area activated by electrodes (compare figure 9(E) and 5(B)). The differences do not arise from mismatched stimulus levels as amplitudes for both modalities were scaled relative to the thresholds determined in the same *in vivo* ECoG recording (compare the peak response amplitudes for figures 5(D) and 9(A)–(D)). Whereas many synaptic pathways and circuits of the brain were necessarily disconnected in the earlier brain slice experiments (Lee *et al* 2016, 2019), the results here suggest that the earlier lack of spread with magnetic stimulation is not simply the result of altered brain structure. The focal confinement of coil-based activation *in vitro* is thought to arise from



the spatially asymmetric fields generated by micro-coils (Lee *et al* 2016, 2019). However, since the magnitude of the induced electric fields are lower than the thresholds thought necessary to activate neurons (Chan and Nicholson 1986), it is likely that the spatial gradient of the fields (activating function) (Maccabee *et al* 1993, Lee *et al* 2016, Lee and Fried 2017) underlie activation. Consistent with this, previous studies suggest that the gradients are supra-threshold in a small region surrounding the coil tip (Lee *et al* 2016). In addition, the (asymmetric) gradients for implanted coils are stronger along the vertical length of pyramidal neurons (vs. along horizontally-oriented passing axons) and thus create a stronger driving force for activation in pyramidal neurons than in passing axons and is thought to help limit activation to only those neurons close to the coil.

Previous studies with micro-coils have shown that responses are sensitive to the orientation between the coil and the long axis of the neuron (Lee and Fried 2017). For example, when the long axis of the coil was parallel to the long axis of targeted pyramidal neurons, a strong spiking response was generated. However, when the long axis of the coil was at an oblique angle (to the long axis of the neuron), spiking was suppressed during stimulation but a burst of activity occurred after stimulation was completed (referred to as an ‘OFF’ response). While care was used to maintain a consistent angle of insertion in the present experiments, the insertion procedure was done by hand and we were not able to observe (or confirm) the resulting insertion angle. Inconsistent insertion angles could explain why some MECP responses had opposite polarities in some of the L2/3 stimulation experiments (positive responses on one side of the coil and negative responses on the other side) (figures 6(D), 7(A) and (B)). The observed asymmetry is potentially interesting because it offers the possibility that activation regions can be further confined, or, even that a single coil could differentially activate

two different regions of cortex, e.g. by varying the polarity of the stimulus current. We did not observe similar negative polarity MECP responses for stimulation of L5. It is not clear why the results differ for the two locations but we note that peak amplitudes of L5 MECPs were smaller than that from stimulation of L2/3 and thus it is possible that the negative polarity responses arising from L5 stimulation were not strong enough to be detected by our recording system. The narrow spatial spread of activation raises questions about whether the elicited response is sufficiently strong to elicit behavioral responses. Similarly, the two polarities of MECPs also may differentially affect elicited visual sensations. While we did not test this here, we found in previous experiments that magnetic stimulation of somatosensory cortex (S1) could drive neural circuits and elicit behavioral responses (whisker movements) with effects that were highly similar to those from electric stimulation (Lee *et al* 2016). We found qualitatively similar results from stimulation of M1 as well. Therefore, it is reasonable to expect that the narrow spread of V1 activation found here will indeed produce meaningful visual stimulation. Further testing will be needed however, to determine whether the opposite polarities in MECPs are both effective.

It is unlikely that responses to stimulation from the coil arose from factors other than inductive activation. We monitored the DC resistance across the coil leads throughout the experiment and they did not change (not shown). Similarly, the impedance from coil to bath ground remained above 200 M $\Omega$  (typically >1 G $\Omega$ ), eliminating the possibility of direct electrical activation. We also monitored the temperature in the bath as well as in the surrounding tissue to ensure that observed responses were triggered by thermal changes (figure 10); temperature increases were typically less than 1 °C, well below the threshold for thermal activation of neurons (Chen *et al* 2015, Eom *et al* 2016). Further, ECoG responses

were weaker when the coil tip was positioned in the deeper layer (L5 vs. L2/3), the opposite of what we might expect if responses were mediated by thermal factors, i.e. thermal increases to be larger for increased coil depths.

### 4.3. Are micro-coils suitable for use in neural prostheses?

The inability to confine activation with electrodes may limit the visual acuity that can be realized with conventional (i.e. electrode-based) cortical implants, e.g. if each electrode must be separated by 2 mm or more to generate non-overlapping phosphenes. There may be a need to separate adjacent electrodes even further when interactions between neighboring electrodes are considered. Interestingly however, Schmidt *et al* (1996) showed that distinct phosphenes can be generated in a human subject for electrode separations as small as 1 mm, raising questions about whether the broad spread of activation shown here and in previous animal studies influences perception. Behavioral testing in animals similarly suggests that the effects of stimulation may be confined to a small region around the electrode, possibly limited to a single cortical column (Tehovnik *et al* 2004), i.e. behavioral responses may arise solely from the stronger activation that occurs locally and less from the sparse activity that spreads well beyond the immediate vicinity of each electrode. This would also be consistent with clinical testing outside the visual system in which electrodes implanted into the hand region of the somatosensory cortex each induced a percept that corresponded reasonably well to its location within the somatic map of S1 (Flesher *et al* 2016). Even stimulating electrodes positioned on the cortical surface (i.e. not implanted into cortex) can create somewhat focal percepts that correspond to the predicted visuotopic map (Beauchamp *et al* 2020), again suggesting that the increased spread of activation may have only a limited effect on the ability to identify and localize phosphenes. Nevertheless, the ability to better confine activation with micro-coils is still likely to be useful for improving the quality of vision elicited by a cortical visual prosthesis. For example, the phosphenes generated by cortical surface stimulation could not be ‘assembled’ into more complex spatial patterns, unless stimulation from each individual electrode was temporally offset (referred to as dynamic stimulation). The need to serially activate electrodes limits the temporal rate at which visual information can be conveyed and may also limit the amount of spatial detail that can be conveyed for a given visual scene. Another challenge with electric stimulation from conventional electrodes is that it triggers strong and long-lasting inhibitory signals that can impede the flow of information through visual pathways (Logothetis *et al* 2010). The ability to better confine activation may help to limit the strength and duration of this inhibition. Finally,

because neighboring pyramidal neurons in V1 typically extract and signal different visual features of the visual scene, stimulation methods that indiscriminately activate a large number of such cells simultaneously produce neural activity that is significantly different from that which arises physiologically; the ability to focally confine activation may thus help to better match the patterns of physiological signaling that arise physiologically, possibly corresponding to an improvement in the quality of elicited vision.

Coil-based cortical implants may also offer enhanced stability compared to conventional (implanted) micro-electrodes. Much previous testing has raised concerns about the long-term stability of electrode-based devices, e.g. higher levels of stimulus current and/or charge density delivered repetitively have been shown to lead to electrode failure over time (Polikov *et al* 2005, Cogan 2008, Cogan *et al* 2016). In addition, implantation into cortex induces a wide range of foreign body responses that can lead to encapsulation of the electrode (McCreery *et al* 2010), potentially altering the effectiveness of stimulation over time (Davis *et al* 2012). The use of inductive activation eliminates the direct interface between metal and brain tissue and therefore reduces a number of concerns related to charge density and its effect on device stability. Also, because magnetic fields pass readily through biological materials, the efficacy of coil-based devices would not be altered by changes to the local environment triggered by implantation, e.g. even severe encapsulation of the implant. Coils can also be insulated with biocompatible materials that have been shown to mitigate some of the cortical responses to implantation (Saxena *et al* 2013, Canales *et al* 2015). Micro-coils may also be an attractive alternative to optogenetic approaches (Arenkiel *et al* 2007, Zhao *et al* 2011) given their ability to selectively target specific cells in a narrow volume of cortex without the need for genetic manipulation. Much additional testing is needed however and the use of specific promoters with optogenetics will likely provide better cell-type specificity.

A significant concern with micro-coils is the high level of stimulus current required to elicit responses. Elevated threshold levels will severely limit the number of independent channels that the prosthesis can support before power demands or heat levels become prohibitive. The low impedance of coils (<10 ohms) vs. that of typical micro-electrodes (~10 k–1 M ohms) will help to mitigate the effects of the high current levels but it will still be highly desirable to reduce the thresholds required for activation. The threshold levels found here (315–472 mA) are considerably higher than those found in previous *in vitro* reports (40–45 mA) (Lee *et al* 2016). Anesthesia is known to disrupt sensory processing in cortex (Lissek *et al* 2016) and so it is possible that the anesthesia protocols used here may have contributed to the high threshold levels. It is also likely that the

inability to optimize the position and the orientation of the coil relative to targeted neurons (as was done in previous *in vitro* experiments) contributed significantly to the higher levels. It is also possible that neural activity close to the coil was indeed evoked by lower amplitudes of magnetic stimulation but that the signal was not strong enough to propagate to the cortical surface, raising the possibility that ECoG measurements may not be an accurate barometer of the actual thresholds. Consistent with some of these concerns, whisker movements in lightly anesthetized mice could be evoked at magnetic stimulation levels as low as 7 mA to 10 mA (Lee *et al* 2016). However, it will be desirable for cortical visual implants to have hundreds or even thousands of independent channels and thresholds of tens or even a few milliamps per channel may still be too high to support safe and effective operation. Behavioral testing in awake behaving animals may confirm that thresholds are indeed lower than those found here and are also likely to provide insight as to whether the ability of coils to better confine activation translates into higher acuity levels and/or other improvements in psychophysical outcomes. Future advances in coil design may also help to reduce power. For example, wireless designs will reduce coil length to 1 or 2 mm with a corresponding reduction in coil resistance (theoretical calculations suggest resistances  $<1 \Omega$ ). Given that the resistance of the coils used in the present study were  $\sim 25 \Omega$ , it is likely that power levels ( $I^2 \times R$ ) will be reduced by a factor of  $\sim 30$ . The use of novel core materials that can greatly intensify field strength e.g. ferrite (Ramrakhyani and Lazzi 2014), mu-metal, and permalloy (Ueno *et al* 1978), may also help to further reduce threshold levels to the point where high-count arrays can be safely implemented.

## Acknowledgments

This work was sponsored by the NIH NEI R01-EY029022 to SWL; the BRAIN Initiative NINDS U01-NS099700 and the Dept. of Defense/CD-MRP (VR170089) to SIF; NSF-CAREER award #1351980, NSF CMMI award #1728497, and NIH DP2-EB029757 to SAD. The authors declare no conflict of interest.

## ORCID iDs

Sang Baek Ryu  <https://orcid.org/0000-0002-1466-871X>

Seung Woo Lee  <https://orcid.org/0000-0003-4070-809X>

## References

- Arenkiel B R, Peca J, Davison I G, Feliciano C, Deisseroth K, Augustine G J, Ehlers M D and Feng G 2007 *In vivo* light-induced activation of neural circuitry in transgenic mice expressing channelrhodopsin-2 *Neuron* **54** 205–18
- Basu I *et al* 2019 Consistent linear and non-linear responses to invasive electrical brain stimulation across individuals and primate species with implanted electrodes *Brain Stimulation* **12** 877–92
- Beauchamp M S, Oswald D, Sun P, Foster B L, Magnotti J F, Niketeghad S, Pouratian N, Bosking W H and Yoshor D 2020 Dynamic stimulation of visual cortex produces form vision in sighted and blind humans *Cell* **181** 774–783 e5
- Bensmaia S J and Miller L E 2014 Restoring sensorimotor function through intracortical interfaces: progress and looming challenges *Nat. Rev. Neurosci.* **15** 313–25
- Borchers S, Himmelbach M, Logothetis N and Karnath H O 2011 Direct electrical stimulation of human cortex - the gold standard for mapping brain functions? *Nat. Rev. Neurosci.* **13** 63–70
- Canales A *et al* 2015 Multifunctional fibers for simultaneous optical, electrical and chemical interrogation of neural circuits in vivo *Nat. Biotechnol.* **33** 277–84
- Chan C Y and Nicholson C 1986 Modulation by applied electric fields of Purkinje and stellate cell activity in the isolated turtle cerebellum *J. Physiol.* **371** 89–114
- Chen R, Romero G, Christiansen M G, Mohr A and Anikeeva P 2015 Wireless magnetothermal deep brain stimulation *Science* **347** 1477–80
- Cogan S F 2008 Neural stimulation and recording electrodes *Annu. Rev. Biomed. Eng.* **10** 275–309
- Cogan S F, Ludwig K A, Welle C G and Takmakov P 2016 Tissue damage thresholds during therapeutic electrical stimulation *J. Neural Eng.* **13** 021001
- Davis T S, Parker R A, House P A, Bagley E, Wendelken S, Normann R A and Greger B 2012 Spatial and temporal characteristics of V1 microstimulation during chronic implantation of a microelectrode array in a behaving macaque *J. Neural Eng.* **9** 065003
- Eom K, Im C, Hwang S, Eom S, Kim T S, Jeong H S, Kim K H, Byun K M, Jun S B and Kim S J 2016 Synergistic combination of near-infrared irradiation and targeted gold nanoheaters for enhanced photothermal neural stimulation *Biomed. Opt. Express* **7** 1614–25
- Fehervari T D, Okazaki Y, Sawai H and Yagi T 2015 *In vivo* voltage-sensitive dye study of lateral spreading of cortical activity in mouse primary visual cortex induced by a current impulse *PLoS One* **10** e0133853
- Fehervari T D and Yagi T 2016 Population response propagation to extrastriate areas evoked by intracortical electrical stimulation in V1 *Front. Neural Circuits* **10** 6
- Flesher S N, Collinger J L, Foldes S T, Weiss J M, Downey J E, Tyler-kabara E C, Bensmaia S J, Schwartz A B, Boninger M L and Gaunt R A 2016 Intracortical microstimulation of human somatosensory cortex *Sci. Transl. Med.* **8** 361ra141
- Franklin K B J and Paxinos G 1997 *The Mouse Brain in Stereotaxic Coordinates* (New York: Academic)
- Ganji M *et al* 2018 Development and translation of PEDOT:PSS microelectrodes for intraoperative monitoring *Adv. Funct. Mater.* **28** 1700232
- Ganji M *et al* 2019 Selective formation of porous Pt nanorods for highly electrochemically efficient neural electrode interfaces *Nano Lett.* **19** 6244–54
- Ganji M, Tanaka A, Gilja V, Halgren E and Dayeh S A 2017 Scaling effects on the electrochemical stimulation performance of Au, Pt, and PEDOT:PSS electrocorticography arrays *Adv. Funct. Mater.* **27** 1703019
- Grill W M, Norman S E and Bellamkonda R V 2009 Implanted neural interfaces: biochallenges and engineered solutions *Annu. Rev. Biomed. Eng.* **11** 1–24
- Hermiz J, Rogers N, Kaestner E, Ganji M, Cleary D, Snider J, Barba D, Dayeh S, Halgren E and Gilja V 2016 A clinic compatible, open source electrophysiology system *Conf. Proc. IEEE Eng. Med. Biol. Soc.* **4511–4**

- Hishida R, Watanabe K, Kudoh M and Shibuki K 2011 Transcranial electrical stimulation of cortico-cortical connections in anesthetized mice *J. Neurosci. Methods* **201** 315–21
- Histed M H, Bonin V and Reid R C 2009 Direct activation of sparse, distributed populations of cortical neurons by electrical microstimulation *Neuron* **63** 508–22
- Keller C J, Honey C J, Megevand P, Entz L, Ulbert I and Mehta A D 2014 Mapping human brain networks with cortico-cortical evoked potentials *Phil. Trans. R. Soc. B* **369** 1–14
- Lee S W, Fallegger F, Casse B D and Fried S I 2016 Implantable microcoils for intracortical magnetic stimulation *Sci. Adv.* **2** e1600889
- Lee S W and Fried S I 2017 Enhanced control of cortical pyramidal neurons with micromagnetic stimulation *IEEE Trans. Neural Syst. Rehabil. Eng.* **25** 1375–86
- Lee S W, T. K and Fried S I 2019 Micro-coil design influences the spatial extent of responses to intracortical magnetic stimulation *IEEE Trans. Biomed. Eng.* **66** 1680–94
- Lewis P M, Ackland H M, Lowery A J and Rosenfeld J V 2015 Restoration of vision in blind individuals using bionic devices: a review with a focus on cortical visual prostheses *Brain Res.* **1595** 51–73
- Lissek T, Obenhaus H A, Ditzel D A, Nagai T, Miyawaki A, Sprengel R and Hasan M T 2016 General Anesthetic Conditions Induce Network Synchrony And Disrupt Sensory Processing In The Cortex *Front. Cell Neurosci.* **10** 64
- Logothetis N K, Augath M, Murayama Y, Rauch A, Sultan F, Goense J, Oeltermann A and Merkle H 2010 The effects of electrical microstimulation on cortical signal propagation *Nat. Neurosci.* **13** 1283–91
- Maccabee P J, Amassian V E, Eberle L P and Cracco R Q 1993 Magnetic coil stimulation of straight and bent amphibian and mammalian peripheral nerve in vitro: locus of excitation *J. Physiol.* **460** 201–19
- Mandonnet E, Winkler P A and Duffau H 2010 Direct electrical stimulation as an input gate into brain functional networks: principles, advantages and limitations *Acta Neurochir.* **152** 185–93
- McCreery D, Pikov V and Troyk P R 2010 Neuronal loss due to prolonged controlled-current stimulation with chronically implanted microelectrodes in the cat cerebral cortex *J. Neural Eng.* **7** 036005
- Minusa S, Osanai H and Tateno T 2018 Micromagnetic stimulation of the mouse auditory cortex *in vivo* using an implantable solenoid system *IEEE Trans. Biomed. Eng.* **65** 1301–10
- Murakami T, Matsui T and Ohki K 2017 Functional segregation and development of mouse higher visual areas *J. Neurosci.* **37** 9424–37
- Normann R A, Greger B, House P, Romero S F, Pelayo F and Fernandez E 2009 Toward the development of a cortically based visual neuroprosthesis *J. Neural Eng.* **6** 035001
- Olsen S R, Bortone D S, Adesnik H and Scanziani M 2012 Gain control by layer six in cortical circuits of vision *Nature* **483** 47–52
- Osanai H, Minusa S and Tateno T 2018 Micro-coil-induced inhomogeneous electric field produces sound-driven-like neural responses in microcircuits of the mouse auditory cortex *in vivo Neuroscience* **371** 346–70
- Oz R, Edelman-klapper H, Nivinsky-margalit S and Slovlin H 2020 Microstimulation in the primary visual cortex: activity patterns and their relation to visual responses and evoked saccades *bioRxiv* 2020 05 03 072322
- Paulk A C et al 2019 Microscale physiological events on the human cortical surface detected with PEDOT:PSS Electrodes *bioRxiv* 770743
- Polack P O and Contreras D 2012 Long-range parallel processing and local recurrent activity in the visual cortex of the mouse *J. Neurosci.* **32** 11120–31
- Polikov V S, Tresco P A and Reichert W M 2005 Response of brain tissue to chronically implanted neural electrodes *J. Neurosci. Methods* **148** 1–18
- Ramrakhiani A K and Lazzi G 2014 Ferrite core non-linearity in coils for magnetic neurostimulation *Healthcare Technol. Lett.* **1** 87–91
- Ryu S B, Werginz P and Fried S I 2019 Response of mouse visual cortical neurons to electric stimulation of the retina *Front. Neurosci.* **13** 324
- Saxena T, Karumbaiah L, Gaupp E A, Patkar R, Patil K, Betancur M, Stanley G B and Bellamkonda R V 2013 The impact of chronic blood-brain barrier breach on intracortical electrode function *Biomaterials* **34** 4703–13
- Schmidt E M, Bak M J, Hambrecht F T, Kufta C V, O’rourke D K and Vallabhanath P 1996 Feasibility of a visual prosthesis for the blind based on intracortical microstimulation of the visual cortex *Brain* **119** 507–22
- Stoney S D JR., Thompson W D and Asanuma H 1968 Excitation of pyramidal tract cells by intracortical microstimulation: effective extent of stimulating current *J. Neurophysiol.* **31** 659–69
- Tehovnik E J, Slocum W M and Schiller P H 2004 Microstimulation of V1 delays the execution of visually guided saccades *Eur. J. Neurosci.* **20** 264–72
- Tehovnik E J, Slocum W M, Smirnakis S M and Tolia A S 2009 Microstimulation of visual cortex to restore vision *Prog. Brain Res.* **175** 347–75
- Tehovnik E J, Tolia A S, Sultan F, Slocum W M and Logothetis N K 2006 Direct and indirect activation of cortical neurons by electrical microstimulation *J. Neurophysiol.* **96** 512–21
- Telfeian A E and Connors B W 1998 Layer-specific pathways for the horizontal propagation of epileptiform discharges in neocortex *Epilepsia* **39** 700–8
- Tolia A S, Sultan F, Augath M, Oeltermann A, Tehovnik E J, Schiller P H and Logothetis N K 2005 Mapping cortical activity elicited with electrical microstimulation using FMRI in the macaque *Neuron* **48** 901–11
- Ueno S, Matsumoto S, Harada K and Oomura Y 1978 Capacitive stimulatory effect in magnetic stimulation of nerve tissue *IEEE Trans. Magn.* **14** 958–60
- Uguz I et al 2016 Autoclave sterilization of PEDOT:PSS electrophysiology devices *Adv. Healthcare Mater.* **5** 3094–8
- Zhao S et al 2011 Cell type-specific channelrhodopsin-2 transgenic mice for optogenetic dissection of neural circuitry function *Nat. Methods* **8** 745–52